Key Points:
- Ambient isoprene mixing ratios observed at 20 sites across China during 2012–2014 are compared with the MEGAN-REAM model simulation
- The model simulated averages in the south were much higher than those in north, while the observed averages were much more similar
- Abnormally high isoprene levels were observed in winter at some northern sites probably due to contributions from nonbiogenic sources

Supporting Information:
- Supporting Information S1

Correspondence to:
X. Wang and Y. Wang,
wangxm@gig.ac.cn;
yuhang.wang@eas.gatech.edu

Isoprene Mixing Ratios Measured at Twenty Sites in China During 2012–2014: Comparison With Model Simulation

Yanli Zhang[1,2,3] (iD), Ruixiong Zhang[4] (iD), Jianzhen Yu[3], Zhou Zhang[1] (iD), Weiqiang Yang[1], Huina Zhang[1], Sujun Lyu[1], Yuesi Wang[5], Wei Dai[6], Yuhang Wang[4] (iD), and Xinming Wang[1,2] (iD)

[1]State Key Laboratory of Organic Geochemistry and Guangdong Key Laboratory of Environmental Protection and Resources Utilization, Guangzhou Institute of Geochemistry, Chinese Academy of Sciences, Guangzhou, China, [2]CAS Center for Excellence in Regional Atmospheric Environment, Institute of Urban Environment, Chinese Academy of Sciences, Xiamen, China, [3]Department of Chemistry, Hong Kong University of Science and Technology, Kowloon, Hong Kong, China, [4]School of Earth and Atmospheric Sciences, Georgia Institute of Technology, Atlanta, GA, USA, [5]State Key Laboratory of Atmospheric Boundary Layer Physics and Atmospheric Chemistry, Institute of Atmospheric Physics, Chinese Academy of Sciences, Beijing, China, [6]Collaborative Innovation Center of Atmospheric Environment and Equipment Technology, Jiangsu Key Laboratory of Atmospheric Environment Monitoring and Pollution Control, School of Environmental Science and Engineering, Nanjing University of Information Science & Technology, Nanjing, China

Abstract Measurement-model comparisons for various atmospheric species have been widely used for evaluating the reliability of model simulations, yet such comparisons are quite limited for atmospheric isoprene due to the lack of systematic observations over a large scale. Here, we collected ambient air samples concurrently at 20 sites in China during 2012–2014 and compared the observed isoprene mixing ratios with those simulated by coupling MEGAN v2.1 with the 3-D Regional chEmical trAnsport Model. The observed average isoprene concentration for all 1,731 samples is 0.35 ± 0.03 ppbv, 13% higher than the model simulated average of 0.31 ± 0.02 ppbv; while during the growing season, the simulated average (0.53 ± 0.05 ppbv) is almost the same as the observed average (0.52 ± 0.04 ppbv). The observed isoprene average level in the north (0.35 ppbv) is similar to that in the south (0.37 ppbv). However, the model simulated average in the south (0.53 ppbv) is ~4 times that in the north (0.14 ppbv). The model overestimated the observations at most southern sites but underestimated at most northern sites in the growing season, which might be resulted from inadequate characterization of isoprene-emitting land vegetation with fast afforestation in the north and rapid urbanization in the south. Compared to the model simulation, the observations revealed abnormally high isoprene levels in winter at some northern sites, largely due to nonbiogenic emissions, as evidenced by the enhancements of measured combustion tracers concurrent with the abnormally elevated isoprene levels.

Plain Language Summary Isoprene alone accounts for approximately one-third of global emission of volatile organic compounds from both nature and human activities, yet in many parts of the world biogenic isoprene emission estimates have large uncertainties (reported isoprene emission estimates span 4–29 TgC y^{-1} in China), and narrowing these uncertainties is a challenging task. Here we collected ambient air samples concurrently at 20 sites over China during 2012–2014, and made measurement-model comparison to check the emission estimates for isoprene, and found that although overall observed and predicted average isoprene levels matched well particularly during growing seasons, there exists a south-north discrepancy that model simulated averages in the south were much higher than the north while their observed averages were quite near each other. Modeled values overestimated at most southern sites but underestimated at most northern sites, probably the fast afforestation in the north and rapid urbanization in the southeast were inadequately characterized in the model. Abnormally higher isoprene levels were observed in winter at some northern sites probably due to contribution from nonbiogenic sources. Our results highlight that high-resolution PFT/LAI, field campaigns with higher spatial and temporal resolutions, as well as biomass burning activity data, are necessary for better observation-model comparison.

1. Introduction

Isoprene (2-methyl-1,3-butadiene, C_5H_8), the biogenic volatile organic compounds (BVOCs) with the highest global emission, represents approximately one third of the global total VOCs emissions and ∼50% of the total BVOCs emissions (Guenther et al., 2006, 2012). Since isoprene is a highly reactive species with an atmospheric lifetime typically less than 1 h (Atkinson & Arey, 1998; Seinfeld & Pandis, 1998), its huge global emission from biogenic sources represents an essential part of land-atmospheric exchange processes, and has profound impacts on atmospheric chemistry and the nature of the atmosphere, such as forming ozone in the presence of nitrogen oxides (NOx) under sunlight (Paulot et al., 2012; Pierce et al., 1998; von Kuhlmann et al., 2004), producing secondary organic aerosols (SOA) (Claeys et al., 2004; Ng et al., 2008; Paulot et al., 2009; Surratt et al., 2010; Ying et al., 2015), and modulating atmospheric oxidation capacity (Butler et al., 2008; Lelieveld et al., 2008; Y. H. Wang et al., 1998). With its great impacts on and complex feedbacks from changes in air quality and climate, isoprene emissions with spatiotemporal resolutions have long been a fundamentally important task for studying regional and global atmospheric processes.

Isoprene emissions algorithms are formulated based on the understanding of leaf- or branch-scale isoprene emissions from various plant types under the influence of environmental factors, such as leaf temperature, photosynthetically active radiation (PAR), humidity, and carbon dioxide (CO_2) concentration (Fehsenfeld et al., 1992; Guenther et al., 1991, 1993). The Model of Emissions of Gases and Aerosols from Nature (MEGAN) is a modeling system for estimating BVOCs emissions from terrestrial ecosystems into the atmosphere (A. Guenther et al., 1995, 2012). The MEGAN model has been widely used to estimate fluxes of BVOCs in terrestrial ecosystems (Kota et al., 2015; P. Wang et al., 2017a), and has also been coupled with land surface and atmospheric chemistry models (Fu & Liao, 2012, 2014; Situ et al., 2014; Tai et al., 2013). Nevertheless, similar to emission inventories for other species, regional or global isoprene emission inventories may be uncertain. Narrowing the uncertainty of emission estimates of BVOCs is highly challenging, and validating the BVOCs emission estimates is a prerequisite for their application and upgrading.

Comparison between simulated and observed ambient concentrations is an approach widely used to validate emission inventories, although this kind of comparison may be biased because model simulated results represent averages over grids and observed results are concentrations merely at a specific sampling site within a grid. For isoprene, such comparison is much more difficult due largely to its high reactivity and the lack of observation data. In the eastern United States (US), where a large amount of isoprene emission occurs, Warneke et al. (2010) found that, compared with measured values, the Community Multiscale Air Quality (CMAQ) embedded with MEGAN with different schemes yielded significantly overestimated isoprene concentrations. Additionally, another study also revealed that MEGAN results tended to overestimate the measured ambient isoprene concentrations (Carlton & Baker, 2011). This is consistent with the over-simulated isoprene concentrations by the MEGAN-CMAQ model in urban areas in southeastern Texas (Kota et al., 2015). A recent study also showed that in the contiguous US, the improved MEGAN model combined with CMAQ can effectively simulate the isoprene concentrations at nonurban sites but not at the urban sites (P. Wang et al., 2017a). Some studies have suggested that anthropogenic sources might contribute to ambient isoprene and lead to the bias between simulated and observed results (Borbon et al., 2001; Park et al., 2011; Song et al., 2008). Kota et al. (2015) and Wang et al. (2017a) demonstrated that the gridded emission factors (EFs), leaf area index (LAI), and PAR values might be the key factors inducing the significant biases between model results and observations. Climatic extremes, such as heatwaves and droughts, may also greatly impact isoprene emissions. A very recent campaign in Wytham Woods in southern England throughout the summer of 2018, which featured a prolonged heatwave and drought, revealed that the model underestimated observations by ∼40% during the heatwave-drought period, and incorporating stress-induced emissions based on leaf temperature and soil water content into current emissions algorithms would lead to significant improvements in model output (Otu-Larbi et al., 2019).

Outside the US and Europe, this kind of comparison between simulated and measured isoprene mixing ratios is very rare, yet the uncertainty in isoprene emission can be even larger in many other regions of the world. Estimates of isoprene emissions in China, for example, span a wide range of 4–29 TgC yr^{-1} in previous studies (Chi & Xie, 2011; Fu & Liao, 2012; A. Guenther et al., 1995; Klinger et al., 2002; L. Y. Li & Xie, 2014; Li et al., 2013, 2020; Tie et al., 2006; Yin et al., 2020). It is under question whether lacking local EFs is an important reason for this large uncertainty, since field campaigns on emission flux measurements
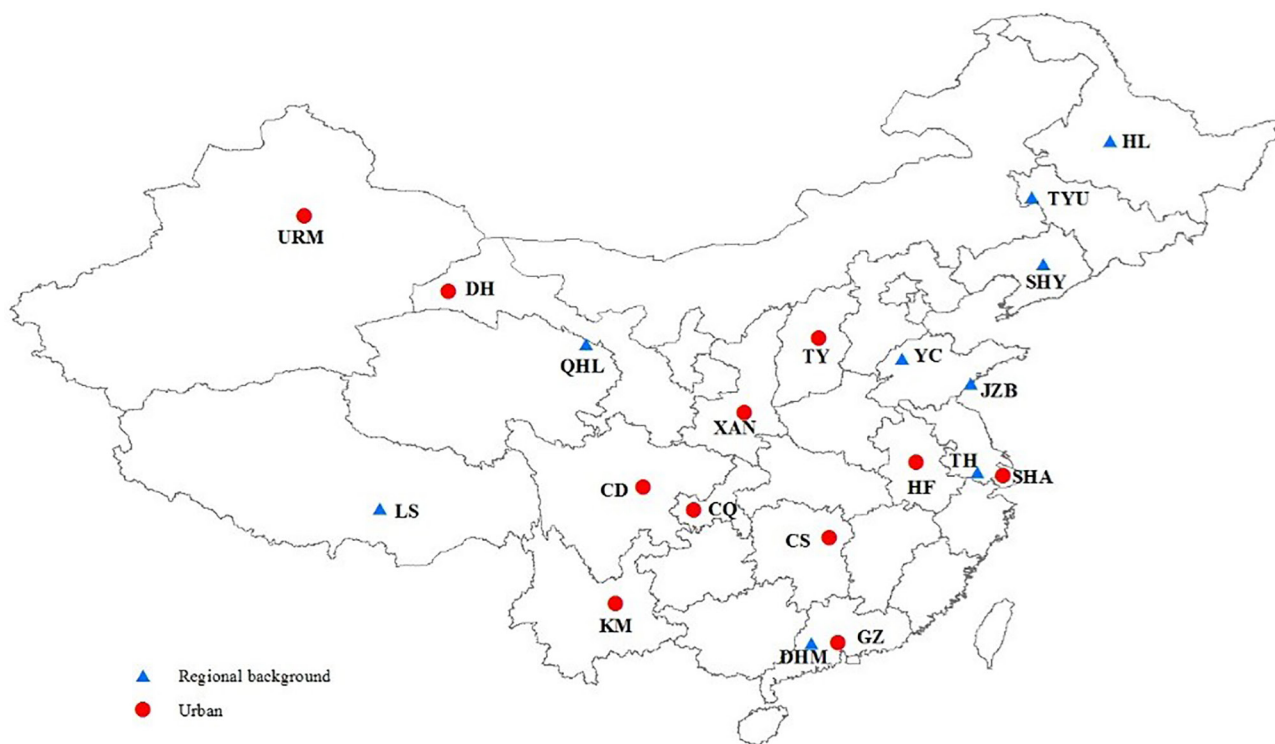
Figure 1. Sampling sites in China, including 11 urban sites (red solid circles): Taiyuan (TY), Hefei (HF), Shanghai (SHA), Changsha (CS), Guangzhou (GZ), Kunming (KM), Chongqing (CQ), Chengdu (Chengdu), Xi'an (XAN), Dunhuang (DH) and Urumchi (URM), and nine regional background sites (blue solid triangles): Hailun (HL), Tongyu (TYU), Shenyang (SHY), Yucheng (YC), Jiaozhou Bay (JZB), Taihu (TH), Dinghu Mountain (DHM), Qinghai Lake (QHL), and Lhasa (LS).

to develop isoprene EFs have mainly been carried out in the developed countries, as summarized in Lathière et al. (2010), and very limited isoprene emission flux measurements have been conducted in China (Bai et al., 2003, 2006, 2015, 2016, 2017; Geron et al., 2006; X. M. Wang et al., 2011). On the other hand, regional surface ozone pollution is a challenging air quality issue in both developed and developing countries (Fujita et al., 2013; Langford et al., 2010; T. Wang et al., 2017b), and isoprene emissions are greatest during the warmer growing season, during which ozone pollution is most probably occurring (T. Wang et al., 2017b). Therefore, for isoprene, which is a very active and effective ozone precursor, the accuracy of its emission estimates is vital in formulating solid ozone control strategies (Chameides et al., 1988; Hewitt et al., 2011; Pierce et al., 1998; Starn et al., 1998).

Considering the tremendously large ranges in isoprene emission estimates and the lack of large-scale long-term observation data for isoprene in China, in the present study, we conducted 2-year concurrent air sampling at 20 sites for ambient isoprene measurement. These observed isoprene mixing ratios were compared with those from model simulation. The study aims to not only provide the spatial and seasonal changes of isoprene in ambient air at representative sites across China, but also evaluate the consistency between model results and observation levels for assessing isoprene emission estimates.

2. Experimental Methodology

2.1. Field Sampling

During the Campaign on Atmospheric Aerosol Research Network of China (CARE-China) (Xin et al., 2015), ambient air samples were collected for the analysis of SOA precursors, including aromatic hydrocarbons (Zhang et al., 2015, 2016a) and BVOCs, at 20 sampling sites, including 9 regional background sites and 11 urban sites across China (Figure 1 and Table 1). Detailed descriptions of each sampling site are provided

Table 1
Description of Sampling Sites

Number	Sampling sites	Abbr.	Type	Longitude	Latitude	Category	Location
1	Hailun	HL	Regional background	126.63°E	47.43°N	NECP	Hailun, Heilongjiang Province
2	Tongyu	TYU	Regional background	122.87°E	44.42°N	NECP	Baicheng city, Jilin Province
3	Shenyang	SHY	Regional background	123.40°E	41.5°N	NECP	Capital city of Liaoning Province
4	Yucheng	YC	Regional background	116.60°E	36.95°N	NCP	Yucheng, Shandong Province
5	Jiaozhou Bay	JZB	Regional background	119.93°E	35.72°N	NCP	Qingdao, Shandong Province
6	Taihu	TH	Regional background	120.22°E	31.40°N	EC	Wuxi, Jiangsu Province
7	Lhasa	LS	Regional background	91.33°E	29.67°N	TP	Capital city of Tibet Autonomous Region
8	Qinghai Lake	QHL	Regional background	101.32°E	37.62°N	NWC	Qinghai Province
9	Dinghu Mountain	DHM	Regional background	112.53°E	23.17°N	SC	Zhaoqing, Guangdong Province
10	Taiyuan	TY	Urban	112.55°E	37.87°N	NCP	Capital city of Shanxi Province
11	Dunhuang	DH	Urban	94.67°E	40.15°N	NWC	Dunhuang, Gansu Province
12	Hefei	HF	Urban	117.27°E	31.86°N	EC	Capital city of Anhui Province
13	Changsha	CS	Urban	113.06°E	28.21°N	SC	Capital city of Hunan Province
14	Chongqing	CQ	Urban	106.54°E	29.59°N	SWC	Chongqing, municipality directly under the central government
15	Kunming	KM	Urban	102.73°E	25.04°N	SWC	Capital city of Yunnan Province
16	Urumchi	URM	Urban	87.68°E	43.77°N	NWC	Capital city of the Xinjiang Uygur Autonomous Region
17	Xi'an	XAN	Urban	108.95°E	34.27°N	NCP	Capital city of Shaanxi Province
18	Guangzhou	GZ	Urban	113.23°E	23.16°N	SC	Capital city Guangdong Province
19	Shanghai	SHA	Urban	121.48°E	31.22°N	EC	Shanghai, municipality directly under the central government
20	Chengdu	CD	Urban	104.06°E	30.67°N	SWC	Capital city of Sichuan Province

in supporting information section 1.1. The nine regional background sites, including Hailun (HL), Tongyu (TYU) and Shenyang (SHY) in the Northeast China Plain (NECP); Yucheng (YC) and Jiaozhou Bay (JZB) in the North China Plain (NCP); Tianhu (TH) in eastern China (EC); Lhasa (LS) in the Tibetan Plateau

(TP); Qinghai Lake (QHL) in northwest China (NWC); and Dinghu Mountain (DHM) in south China (SC), are all ecosystem research stations established in the Chinese Ecosystem Research Networks (http://www.cern.ac.cn/0index/index.asp/). These stations are all located in rural/forest/remote areas with few human activities in their neighboring areas. The 11 urban sites (except Dunhuang) are all located in China's provincial capital cities/municipalities directly under the Central Government including Guangzhou (GZ) and Changsha (CS) in SC; Kunming (KM), Chengdu (CD), and Chongqing (CQ) in southwest China (SWC); Shanghai (SHA) and Hefei (HF) in EC; Taiyuan (TY) and Xi'an (XAN) in NCP; Urumchi (URM) and Dunhuang (DH) in NWC.

Ambient air samples were collected concurrently at the 20 sampling sites at approximately 14:00 Beijing time (6:00 UTC) every Wednesday from March 2012 to April 2014. Ambient air was compressed into cleaned and evacuated 1 L Silonite-treated stainless canisters (Entech Instruments Inc.,) to ∼30 psi over approximately 60 min using highly purified oil-free pumps. A total of 1731 samples were collected at the 20 sampling sites. The samples were all directly transported back to the laboratory at Guangzhou Institute of Geochemistry to measure VOCs, including isoprene. A detailed description of the field works can be found elsewhere (Xin et al., 2015; Z. Zhang et al., 2015, 2016b).

2.2. Laboratory Analysis

The air samples were analyzed with a Model 7100 Preconcentrator (Entech Instruments Inc.,) coupled with an Agilent 5973N gas chromatography-mass selective detector/flame ionization detector/electron capture detector (GC-MSD/FID/ECD, Agilent Technologies). The detailed cryogenic concentration steps are described elsewhere (Y. L. Zhang et al., 2012, 2013). Briefly, 500 mL air samples were drawn through a liquid-nitrogen cryogenic trap (1/8 inch × 20 cm) with glass beads (60/80 mesh) at −160°C. After trapping, this primary trap was heated to 10°C, and all target compounds were transferred by pure helium to the secondary trap (1/8 inch × 20 cm) at −50°C with Tenax-TA (60/80 mesh) as an adsorbent. The redundant H_2O and CO_2 were mostly removed through this micro-Purge-and-Trap step. The secondary trap was then heated, and the VOCs were transferred by helium to a third cryo-focus trap (1/32 inch × 5 cm) at −170°C. After the focusing step, the trap was rapidly heated, and the VOCs were transferred to the GC-MSD/FID/ECD system. The mixture was first separated by a DB-1 capillary column (60 m × 0.32 mm × 1.0 μm, Agilent Technologies), with helium as the carrier gas at a constant rate of 4.0 ml/min, and then split into three ways controlled by a splitter to a 0.35 m × 0.10 mm interior diameter (I.D.) stainless steel line output to the MSD, to a 0.35 m × 0.10 mm I.D. stainless steel line output to the ECD, and to an HP PLOT-Q column (30 m × 0.32 mm × 20.0 μm, Agilent Technologies) output to the FID. The GC oven temperature was programmed to be initially at 10°C, which was held for 3 min, then increased to 120°C at 5°C/min, and then to 250°C at 10°C/min with a final hold time of 20 min. The MSD was operated in selected ion monitoring (SIM) mode, and the ionization method was electron impacting.

2.3. Quality Control and Quality Assurance

Before sampling, all canisters were cleaned at least five times by repeated filling and evacuating of humidified zero air. To check if there was any contamination in the canisters, all vacuumed canisters, after the cleaning procedure, were re-filled with humidified zero air and stored in the laboratory for at least 24 h, and then analyzed by the same methods as the field samples, thus, ensuring that none of the target VOC compounds were present.

Target compounds were identified based on their retention times and mass spectra and were quantified by external calibration methods. The calibration standards were prepared by dynamically diluting the PAMS standard mixture and TO-14 standard mixture (100 ppbv, Spectra Gases Inc.,) to 0.5, 1, 5, 15, and 30 ppbv, respectively. The calibration curves were obtained by running the five diluted standards, plus the humidified zero air, the same manner as the field samples. Each day, before sample analysis, the analytical system was checked initially with humidified zero air to ensure that it was clean, and then with a one-point (typically 1 ppbv) calibration. If the response was beyond ±10% of the initial calibration curve, recalibration was performed.

2.4. Model Simulation of Isoprene Mixing Ratios (MEGAN and 3D-REAM Model)

The isoprene mixing ratios were simulated by coupling MEGAN v2.1 (A. B. Guenther et al., 2012) and the 3-D REAM (R. X. Zhang et al., 2017), which has been used in previous studies for transport processes, emission estimates and air quality studies. The MEGAN model uses satellite-retrieved LAI and plant functional type (PFT) data from the Moderate Resolution Imaging Spectroradiometer (MODIS) and the Advanced Very High Resolution Radiometer, prepared for year 2003 (http://www2.acom.ucar.edu/wrf-chem/wrf-chem-tools-community, last accessed at November 25, 2019) and 2000 (A. Guenther et al., 2006), respectively. We use 1 km resolution MODIS data of the study years to compute the base isoprene emissions (at standard light and temperature conditions) in each model grid cell. The EFs for specific PFTs are from Guenther et al. (2012) using MEGAN2.1 algorithms in Community Land Model (CLM4) for year 2000. The PFT types used for the 20 sampling sites were shown in Table S2. MEGAN-REAM simulated isoprene emissions in China for June–July–August in 2013 are shown in Figure S1 as an example. Anthropogenic emissions from the Multiresolution Emission Inventory for China (MEICv1.2, M. Li et al., 2017) for year 2012 were used in all model simulations. The speciated nonmethane VOC emissions for SAPRC-99 and CB05 mechanisms were developed by Tsinghua University following a profile-assignment approach. Monthly gridded emissions at a spatial resolution of $0.25 \times 0.25°$ are available and can be accessed from http://www.meicmodel.org/ (M. Li et al., 2017). MEIC estimates anthropogenic isoprene emissions from industry, transportation, and residential sources. However, they are of high uncertainty and more importantly, they are 2–3 orders of magnitude lower than natural emissions estimated by MEGAN. Therefore, the inclusion of the negligible anthropogenic isoprene sources in MEIC would have little influence on our conclusions, and we only include natural isoprene emissions in our simulations.

Detailed information about REAM can be found elsewhere (Choi et al., 2008a, 2008b; J. Li et al., 2019; Y. Zhang et al., 2016a; R. X. Zhang et al., 2017, 2018; Zhao et al., 2010) and the references therein. Briefly, REAM has a horizontal resolution of 36×36 km with 30 vertical layers in the troposphere and five vertical levels in the stratosphere covering China and its adjacent regions. The model meteorological fields are hourly averages of the 5-min outputs from the Weather Research and Forecasting (WRF) model assimilation constrained by National Centers for Environmental Prediction Climate Forecast System Reanalysis (NCEP CFSR; Saha et al., 2010) 6-hourly products, which have a horizontal resolution of T382 ($\sim$38 km). The REAM isoprene-related chemical mechanism expands the GEOS-Chem standard chemical mechanism (V9-02) to include a detailed description of aromatic chemistry (Bey et al., 2001; Liu et al., 2010, 2012a, 2012b; R. X. Zhang et al., 2017).

2.5. Model Sensitivity Tests

The REAM model was once applied to simulate aircraft observations over the Washington-Baltimore area during the field campaign of Deriving Information on Surface Conditions from Column and Vertically Resolved Observations Relevant to Air Quality (DISCOVER-AQ). In summer 2011, high concentrations of isoprene, 2–3 ppbv in the lower boundary layer, were observed in this field campaign. In total, >250 vertical profiles of aircraft measurements were previously simulated by the REAM model, and the simulated isoprene (as well as ozone and NOx) concentrations were in good agreement with the observations (Cheng et al., 2017; Y. Zhang et al., 2016a; Figure S2). To provide a rough estimate of the model performance against the observations, we provide comparisons between model simulations in this research and satellite NO_2 observations in China in the supplement (supporting information section 1.2). We do not find observation evidence or have plausible reasons to suspect that the model simulations have a north-to-south bias.

Furthermore, we performed sensitivity tests of simulated isoprene in response to the changes of NO_x emissions and planetary boundary layer height (PBLH) during June–July–August of 2013. We increased the PBLH by one vertical layer at the top of the PBL in the model, corresponding to an increase of the PBLH by 15%–30%. The simulated isoprene concentrations with increasing PBLH were about 5% lower than the standard simulations (Figure S3). The relatively low sensitivity of simulated isoprene to the PBLH increase manifested the short lifetime of atmospheric isoprene because of its high reactivity (Y. Zhang & Wang, 2016). We also decreased NO_x emissions by 20% in another sensitivity study and found that the surface isoprene change was generally within $\pm10\%$ (Figure S3). The relative changes of OH concentrations and isoprene concentrations varied across sites with the uniform 20% decrease of the NO_x emissions due
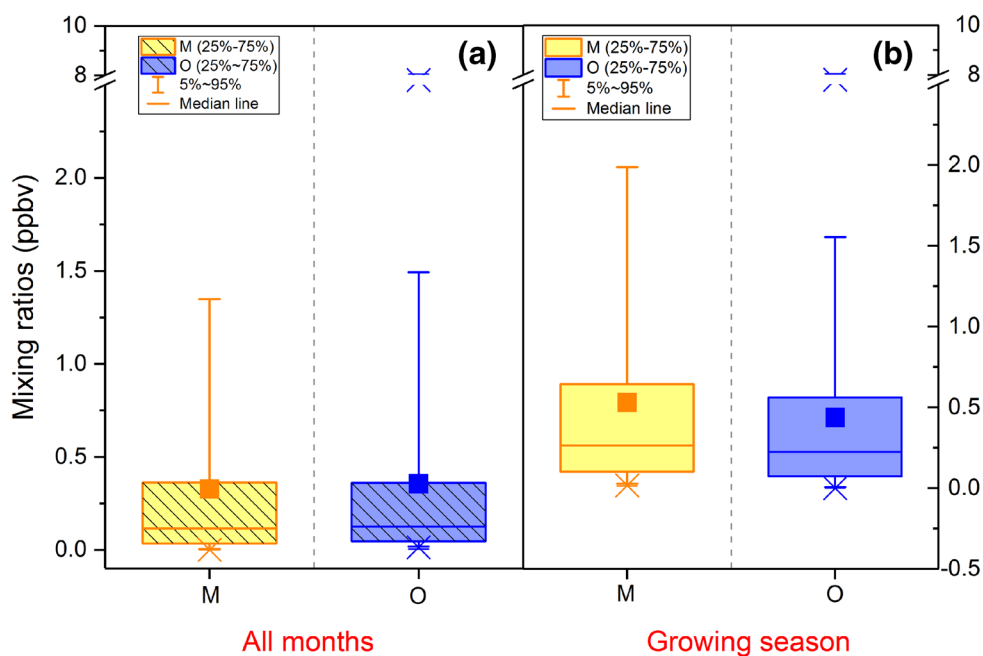
Figure 2. Comparison of isoprene mixing ratios between model simulation and ambient observation at 20 sites for 2 years: (a) all month averages and (b) growing-season (May–October) averages.

in part to chemical nonlinearity (Z. Liu et al., 2012a). These sensitivity simulations implied that moderate changes of PBL and NO_x emissions could not explain the large north-south discrepancies between simulated and observed isoprene concentrations found in this study. Therefore, the uncertainty in the isoprene emissions may contribute the most to the uncertainties in the isoprene simulation (L. Li et al., 2020; Yin et al., 2020).

3. Results and Discussion

3.1. Overview of Observed and Simulated Average Isoprene Mixing Ratios

A comparison of ambient isoprene mixing ratios between our measurements and the measurements made in other studies in China is presented in SI. Based on our 2-year concurrent observations at 20 stations across China, the average mixing ratio of isoprene was 0.35 ± 0.03 ppbv (average $\pm 95\%$ confidence interval, C.I.) (Figure 2a). The lowest annual average, 0.07 ± 0.03 ppbv, was observed at the regional background site LS in the TP, while the highest annual average, 0.72 ± 0.31 ppbv, was observed at the urban site XAN in the NCP region. The Qinling Mountains-Huaihe River Line is widely used as the geographical south-north dividing line in China due to differences in climate, plant types, agricultural activities, etc. (Wei et al., 2014). The 20 sites can be categorized into the north and the south groups: the north group includes the 10 sites in the NECP, NCP, and NWC regions, and the south group includes 9 sites in the EC, SC, and SWC regions. LS is included in neither group due to its unique location in the TP. To our surprise, there is no significant difference in average mixing ratios between the north group (0.35 ± 0.05 ppbv) and the south group (0.37 ± 0.05 ppbv). The average mixing ratio of isoprene simulated by the MEGAN-REAM model during the same time intervals as field sampling at the 20 sites was 0.31 ± 0.02 ppbv (Figure 2a), which is approximately 11% lower than that of 0.35 ± 0.03 ppbv from the observations. Unlike the observation results with the similar north-south average mixing ratios, the simulated average for the south (0.53 ± 0.05 ppbv) was ~4 times of that for the north (0.14 ± 0.02 ppbv).

As isoprene emissions display distinct seasonal variations (A. B. Guenther et al., 1993; Situ et al., 2013) with levels that are typically much higher during the growing season (May–October), the mixing ratios of isoprene based on model simulation and field observations during the growing season were further compared. As shown in Figure 2b, the simulated average mixing ratio of isoprene is 0.51 ± 0.04 ppbv during
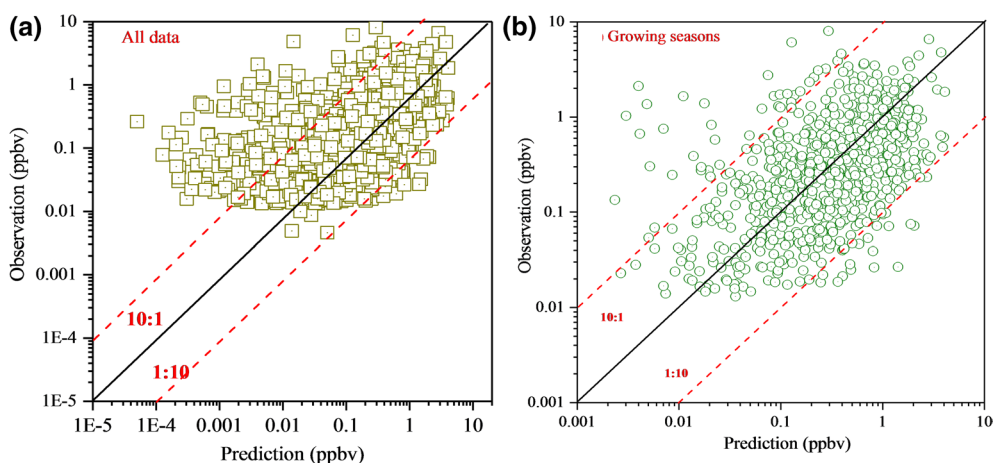
Figure 3. Observed versus simulated isoprene mixing ratios for (a) all month and (b) growing season (May–October).

the growing season, which is very similar to the observed average of 0.53 ± 0.05 ppbv. The observed and simulated average mixing ratios of isoprene during the growing season were 1.5 and 1.7 times of these for all months, respectively. Similar with the annual average, no significant difference was found between the south group (0.58 ± 0.08 ppbv) and the north group (0.53 ± 0.08 ppbv) for the observed average isoprene levels during growing season. In contrast, the average levels of isoprene in south group (0.86 ± 0.07 ppbv) were ∼3.4 times of that in north group (0.25 ± 0.03 ppbv) from the model simulation results. If the 20 sites were further categorized into urban and regional background ones (Table 1), the measurement-model comparisons revealed fairly good model performances: during the growing seasons, modeled average isoprene mixing ratio for the urban group (0.62 ppb) was only ∼5% less than that observed (0.65 ppb), while modeled average isoprene mixing ratio for the regional background group (0.42 ppb) was exactly matched that observed (0.42 ppb); even for the whole year, the measurement-model differences in average isoprene mixing ratios were all within 10% either for the urban group or for the regional background group.

The scatter plots of the observed and simulated isoprene mixing ratios (Figure 3) imply that the simulated values match the observed values much better during the growing season than during the other months. Furthermore, Figure 3a demonstrates that for quite a lot of samples, the differences between the observed and simulated isoprene mixing ratios were more than one order of magnitude; that is, the dots plotted beyond the 10:1 or 1:10 lines in the scatter plot. Even in the growing season, ∼8% of the samples did not fall between the 10:1 and 1:10 lines, with simulated/observed differences exceeding one order of magnitude (Figure 3b).

3.2. Simulated and Observed Isoprene Mixing Ratios During the Growing Season in Different Regions

As plant types in China vary largely both from north to south and from east to west (J. Y. Fang et al., 2002; and the references therein), the observed and simulated results in different regions were investigated during the growing season when biogenic isoprene emissions mostly occur. According to the major PFTs in China shown in Fu and Liao (2012), the 20 sampling locations can be grouped into 7 regions, namely NECP, NCP, NWC, EC, SC, SWC, and TP. Figure 4 shows the means and medians of the observed and simulated isoprene levels in the seven regions during the growing season.

The highest observed and simulated mixing ratios of isoprene both occurred in the SC region, with the average of simulated levels (1.41 ± 0.15 ppbv) being ∼1.8 times of the measured results (0.77 ± 0.16 ppbv). Similar over-prediction also occurred in the EC region, with simulated levels of 0.57 ± 0.08 ppbv, which is also ∼1.8 times the observed value of 0.31 ± 0.05 ppbv. The over-prediction of isoprene mixing ratios at SHA and TH, two sites located in the Yangtze River Delta (YRD), is consistent with a very recent study carried out in the YRD, which showed that PFT type based on MODIS may overestimate isoprene emission by 66% (Y. Wang et al., 2020). Furthermore, Wang et al. (2020) also illustrated that PFT had a greater impact on the
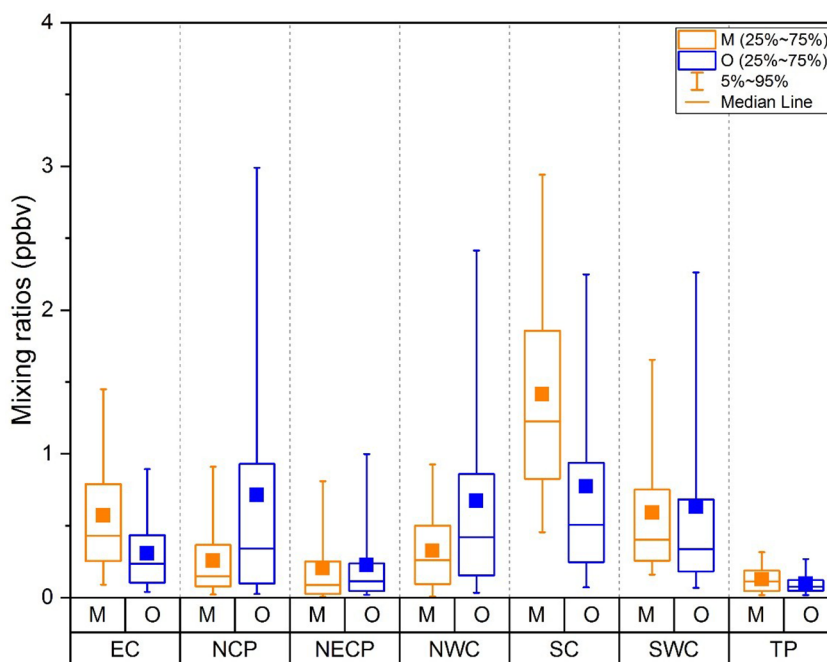
Figure 4. Comparison of isoprene mixing ratios between model simulation and ambient observation in different regions during growing season (May–October).

amount and spatial distribution of the isoprene emission than emission factor through the tests of three land cover datasets across the YRD region. In contrast, the simulated levels in the NCP (0.26 ± 0.14 ppbv) and NWC (0.33 ± 0.01 ppbv) regions were 64% and 52% lower, respectively, than the observed values. The simulated results in the NECP and SWC regions, however, seemed to be highly consistent: the isoprene levels observed in the NECP, SWC, and TP regions were 0.23 ± 0.06 ppbv, 0.63 ± 0.16 ppbv, and 0.10 ± 0.02 ppbv, while their simulated counterparts were 0.20 ± 0.05 ppbv, 0.59 ± 0.08 ppbv, and 0.13 ± 0.02 ppbv, respectively.

This region-specific model performance can also be seen in the scatter plots between the observed and simulated values (Figures 5 and S4). Relatively good agreements between simulated and observed isoprene levels were found in the SWC and TP regions, with 92% and 86% of the results lying between the 1:4 and 4:1 lines, and moderate agreements were found in the NWC regions, with 75% of the results lying between the 1:4 and 4:1 lines. In other regions, only 65%–69% of the results fell between the 1:4 and 4:1 lines. The rooted mean squared error (RMSE) is a frequently used measure of the differences between predicted and observed values and gives relatively high weight to large errors. The lowest RMSE (0.12) between the observed and predicted isoprene values was found in the TP region, while the highest RSME (1.2) was found in the SC region.

3.3. Site-specific Differences Between Observed and Simulated Levels

Figure 6 shows the spatial variations in the simulated and observed average levels of isoprene at the 20 sites during the growing season (Table 2). The best measurement-model consistency occurred at CQ, with a difference between the simulated value (0.95 ± 0.15 ppbv) and the observed value (0.91 ± 0.21 ppbv) of less than 5%. Fairly good measurement-model consistency also occurred at HF and KM with differences of less than 30%. The simulated results showed underestimation for most of the sites located in the north but overestimation for most of the sites in the south.

The largest underestimates occurred at QHL in the NWC region, with simulated values (0.06 ± 0.03 ppbv) 88% lower than the observation values (0.51 ± 0.25 ppbv), and at YC in the NCP region, with simulated values (0.12 ± 0.02 ppbv) 84% lower than the observations (0.75 ± 0.29 ppbv) on average. The mean isoprene
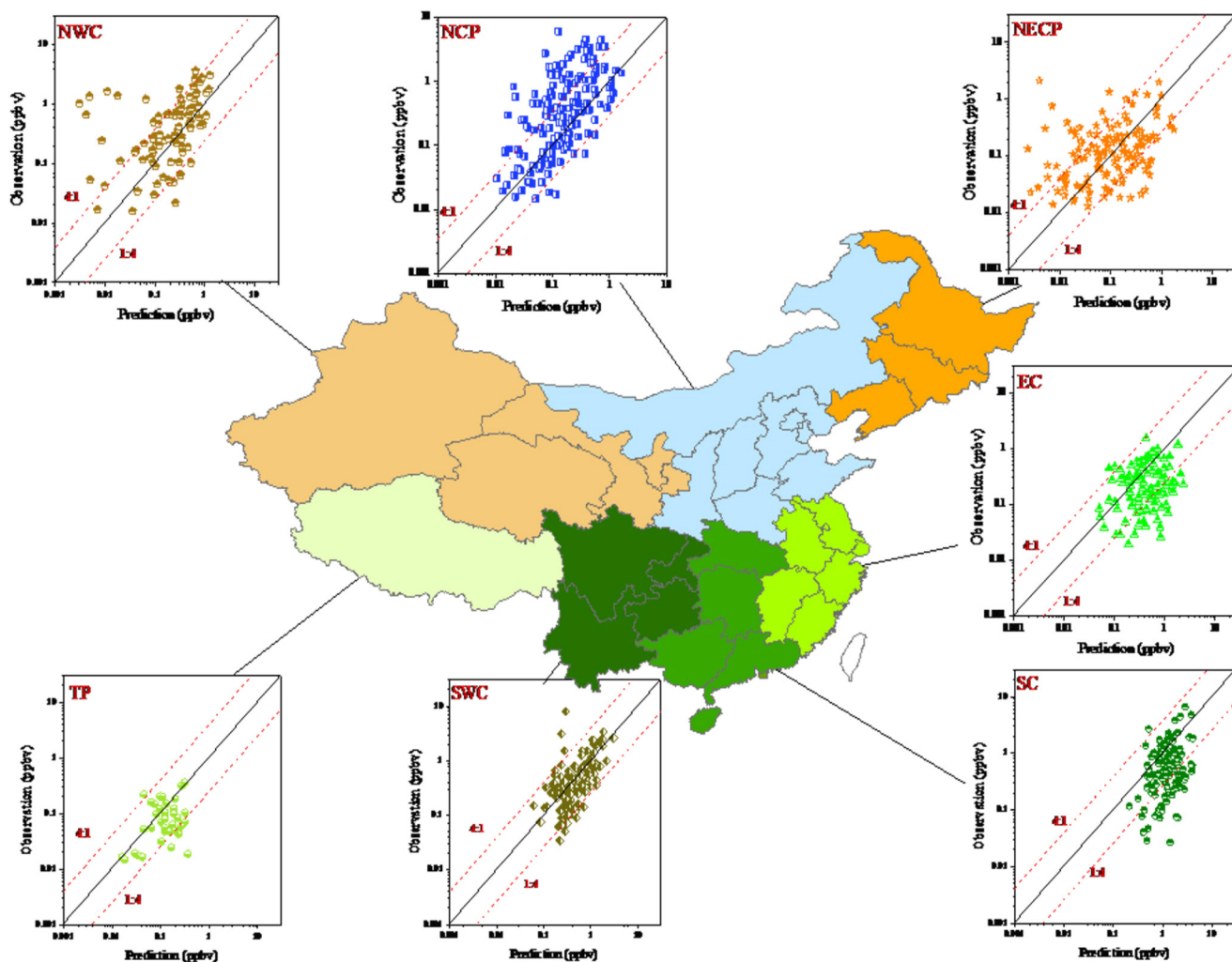
Figure 5. Observed versus simulated isoprene mixing ratios during growing season in different regions.

mixing ratio in the growing season at DH from the model simulation (0.41 ppbv) was significantly lower than that from the observations (0.88 ppbv). In fact, many studies demonstrated that human land cover change has dominated BVOC emission variability over the past years on a global scale (Arneth et al., 2011; Hantson et al., 2017; Henrot et al., 2017; Lathière et al., 2010; Unger, 2013, 2014). The localized emission factors and different PFT distributions are the most important factors influence the isoprene emission on regional scales (L. Li et al., 2020; X. M. Wang et al., 2011, 2018a, 2020). A recent study showed that the global leaf area increased by 2.3% per decade from 2000 to 2017, in which China alone accounts for 25% of the global net increase in leaf area mainly due to forest conservation and tree planting particularly in north China (C. Chen et al., 2019). The fractions of land covered by forests exhibited increases in northeastern China by 5%–15% from the late 1980s to the mid-2000s (Fu & Liao, 2014). The 5%–10% increments of isoprene emissions were also found in Northeast China and India because of afforestation efforts by the study of Chen et al. (2018). In the Loess Plateau in northwest China, the area of forest increased 48,786 km^2 from 2001 to 2016, with the percentage of forested areas changing from 8.19% to 15.82% (Y. Wang et al., 2018b). A recent study revealed increased emissions of isoprene from 2008 to 2018 in most north regions of China but reduced emissions in most south regions of China (L. Li et al., 2020), largely due to the changes of broadleaf trees with higher isoprene emission potentials. Thus, a growth of afforestation or a rapid increase in vegetated areas in the north regions might be a reason for the underestimation.
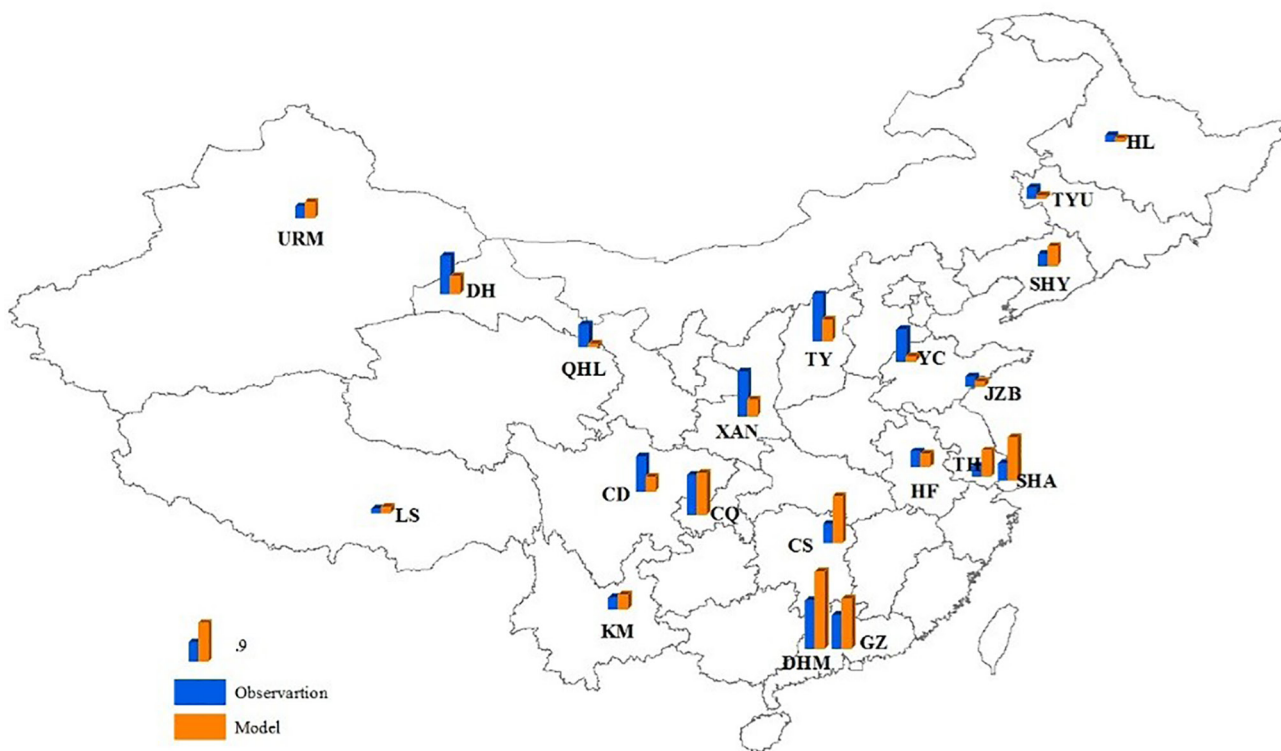
Figure 6. Spatial variations of average mixing ratios of isoprene at the 20 sites during growing season (May–October).

The largest over-prediction occurred at SHA, TH, and CS, where the simulated values of 1.00 ± 0.25, 0.60 ± 0.11, and 1.09 ± 0.16 ppbv were all over two times higher than the observed values of 0.38 ± 0.64, 0.23 ± 0.06, and 0.43 ± 0.09 ppbv, respectively. These sites are located in some of China's megacities, and part of the over-predictions at these sites might also be related to rapid urbanization rates in the regions. In recent decades, the scale of urbanization in China has been unprecedented in human history. The degree of urbanization in China grew from 46.99% in 2008 to 59.58% in 2018, with an average annual increase rate of more than 1% (Zhou et al., 2020). The total urban area in the mid-2000s was four times that in the late 1980s (Fu & Liao, 2014). Moreover, China's urbanization rates are much faster in the southeast than in the northwest. As an example, In Guangdong Province in south China, the urbanized area was 17.4% in 1980, but it increased to 68.7% in 2015, this urbanization rate is much faster than most of the regions in north China (Yan et al., 2020). Wang et al. (2011) showed large difference of isoprene emissions estimation between the application of local-surveyed PFTs and MODIS PFTs in 2006. Therefore, if the land-use change is not duly updated in the regions with rapid urbanization rates, land cover by vegetation would be overestimated, the emissions and mixing ratios of BVOCs might therefore also be overestimated.

From the detailed measurement-model comparisons during the growing season at each site (Figure S4), the better consistency occurred at the CQ, KM, and HF sites, with over 90% of the results lying between the 1:4 and 4:1 lines and having relatively low RMSE values (<0.62). Good model performance was also found at the CD, LS, DH, URM, and XAN sites, with more than 80% of the results lying between the 1:4 and 4:1 lines and having RMSE values with a range of 0.12–1.67. Relatively worse performance was found at QHL in the NWC region, with only 40% of the results lying between the 1:4 and 4:1 lines.

3.4. Differences in Monthly Variations Between Observed and Simulated Levels

As mentioned before, this kind of measurement-model comparison may be biased because the model simulated results represent averages in grids, while the observed results represent the concentrations at a

Table 2
Isoprene Mixing Ratios (ppbv) During the 2-years Campaign and in Growing Season at the 20 Sampling Sites

	Two years				Growing season			
	Observation		Prediction		Observation		Prediction	
Sampling sites	Mean	95% C.I.	Mean	95% C.I.	Mean	95% C.I.	Mean	95% C.I.
HL	0.11	0.03	0.04	0.01	0.14	0.05	0.07	0.02
TYU	0.25	0.07	0.04	0.01	0.26	0.11	0.07	0.02
SHY	0.23	0.07	0.24	0.06	0.27	0.11	0.43	0.10
YC	0.51	0.20	0.07	0.01	0.75	0.29	0.12	0.02
JZB	0.15	0.04	0.06	0.02	0.23	0.06	0.11	0.03
TH	0.15	0.04	0.35	0.07	0.23	0.07	0.60	0.11
LS	0.07	0.02	0.07	0.02	0.10	0.02	0.13	0.02
QHL	0.36	0.15	0.05	0.02	0.51	0.25	0.06	0.03
DHM	0.64	0.20	1.17	0.18	1.12	0.34	1.80	0.25
TY	0.62	0.21	0.27	0.07	1.10	0.33	0.51	0.10
DH	0.52	0.16	0.23	0.06	0.88	0.23	0.41	0.09
HF	0.22	0.04	0.16	0.04	0.36	0.07	0.30	0.06
CS	0.28	0.06	0.69	0.12	0.43	0.09	1.09	0.16
CQ	0.53	0.13	0.57	0.11	0.91	0.21	0.95	0.15
KM	0.22	0.04	0.27	0.04	0.27	0.05	0.35	0.04
URM	0.20	0.05	0.16	0.06	0.27	0.08	0.37	0.10
XAN	0.72	0.31	0.19	0.06	1.05	0.50	0.39	0.10
GZ	0.58	0.21	0.62	0.17	0.79	0.27	1.17	0.22
SHA	0.29	0.11	0.51	0.17	0.38	0.17	1.00	0.25
CD	0.52	0.35	0.22	0.06	0.81	0.64	0.35	0.09

Abbreviations: CD, Chengdu; CS, Changsha; CQ, Chongqing; DHM, Dinghu Mountain; DH, Dunhuang; GZ, Guangzhou; HL, Hailun; HF, Hefei; JZB, Jiaozhou Bay; KM, Kunming; LS, Lhasa; QHL, Qinghai Lake; SHA, Shanghai; SHY, Shenyang; TH, Taihu; TYU, Tongyu; URM, Urumchi; XAN, Xi'an; YC, Yucheng.

specific sampling site within a grid. Furthermore, the deviation of simulated results might also come from inaccurate local isoprene emissions and/or simulated meteorology. The WRF simulation at 36 km resolution might be insufficient to capture air mass transport. However, the major factors influencing isoprene emissions, such as sunlight and temperature, can be reasonably considered as the same within a grid cell, and they regulate isoprene emissions from different plant types in a similar manner. Therefore, even if the model results may fail to match the observed results due to the choice of sampling site within a grid cell, the model should still reproduce the change in biogenic isoprene concentrations as a function of vegetation growth, light, and temperature.

Due to the dependence of isoprene emissions on solar radiation and temperature, the maximum emissions from plants and ambient concentrations of isoprene normally occurred in summer, and the minimum emissions occurred in winter (Fu & Liao, 2012; A. Guenther et al., 1995). The observed and simulated monthly variations in isoprene at 20 sites are presented in Figure 7 and Figures S5–S9. Based on the model simulation, the highest levels of isoprene reasonably occurred in summer and the lowest in winter for all sites, with Gaussian distribution-like shapes from January to December. The highest observed mixing ratios of isoprene also occurred in the growing season at all the sites except KM, but the observed values showed larger monthly fluctuations than the simulated results. At the KM site, the highest monthly average occurred in April, with the relatively high mixing ratios of isoprene observed in the third (1.10 ppbv) and the 4th week (1.31 ppbv) of April in 2014. The monthly variations in the observed and simulated isoprene levels showed similar trends at YC, TY, XAN, QHL, DH, and CD sites, but the simulated monthly average mixing
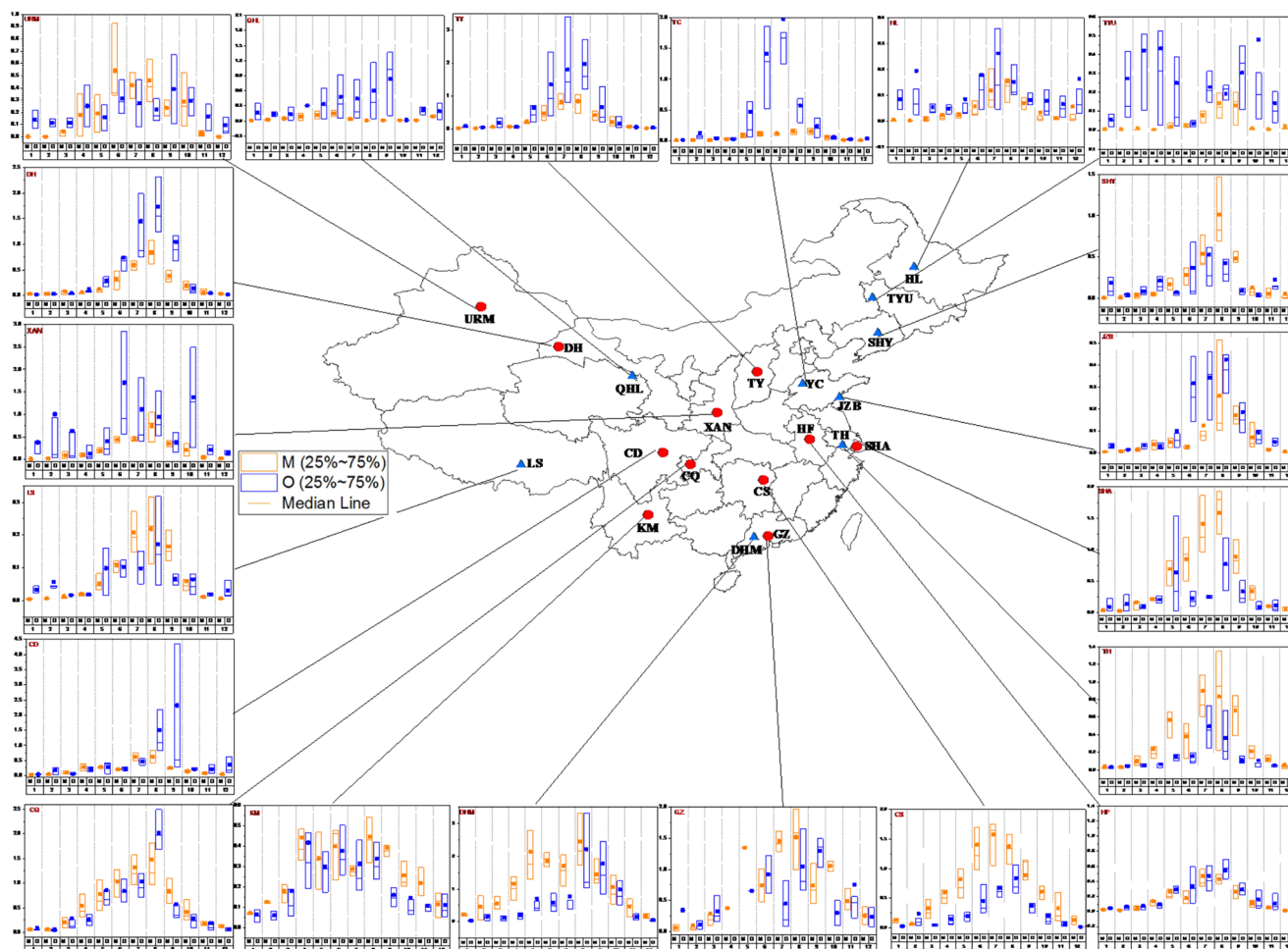
Figure 7. Comparison of monthly variations of isoprene mixing ratios between model simulation and ambient observation at the 20 sites.

ratios were all lower than the observed values. In contrast, the simulated monthly average mixing ratios of isoprene during the growing season were much higher than the observed values at SHA, TH, CS, GZ, DHM, and CQ sites, which caused the simulated 2-year average levels of isoprene at these sites to be larger than the observed values.

The comparison of observed and simulated results at the 20 sites revealed better agreement in the monthly variations at sites in the SC, SWC, and EC regions than at the sites in the other regions. At the sites in the NECP, NCP, and NWC regions in northern China, the simulated results all underestimated the observations except at SHY. Noticeably, comparatively higher mixing ratios were observed during the nongrowing season at the NECP, NCP, and NWC regions, especially at the HL, TYU, XAN, and URM sites. This indicates that there might be isoprene sources other than natural emissions, such as biomass/biofuel burning or coal burning. At the HL site, for example, a significant enhancement of isoprene was observed during winter (such as January 2012, December 2013, and January 2014) when elevated mixing ratios of combustion source markers, including carbon monoxide, benzene, acetylene, and methyl chloride (C. Liu et al., 2017a; Simpson et al., 2011; Zhang et al., 2012, 2013), were also observed (Figure S10), suggesting that the enhancement of isoprene during wintertime might be related to combustion sources. Similar model under-prediction was also observed at other sites, such as TYU (Figure S11). In fact, isoprene emissions from combustion sources have been reported previously. Li et al. (2019) and Simpson et al. (2011) revealed that the open burning of agricultural residues or forest fires could also emit isoprene to the atmosphere. A recent study demonstrated that open burning of wheat, corn, and rice residues had EFs of up to ~0.1 g kg^{-1} (Z. Fang et al., 2017). Andreae (2019) recently updated the emission factor of a wide spectrum of chemicals, including isoprene,

from various types of biomass burning, and isoprene was detected in emissions from all kinds of burned biomass, including crop residues, coals, biofuels and woods, with EFs ranging 0.07–0.52 g kg^{-1}. In northern China, coal and biomass are widely used for household heating in wintertime (C. Liu et al., 2017b; Yang et al., 2018); therefore, isoprene from these combustion sources would lead to higher isoprene mixing ratios than those simulated by the model, because natural isoprene emissions that are only considered by the model are usually negligible during winter in the north China. Including the longer-lived isoprene oxidation products such as methacrolein and methyl vinyl ketone may improve the model evaluations of isoprene sources although the uncertainties in the yields of these isoprene oxidation products need to be taken into account.

4. Conclusions

In this study, we carried out 2-year (2012–2014) concurrent observations of ambient isoprene at 20 sites across China and compared the measured isoprene mixing ratios with those simulated by coupling MEGAN v2.1 with the 3-D REAM model to reveal the uncertainty of model simulation about isoprene emission estimates. On the national scale, the average isoprene mixing ratio from the model simulation showed fairly good consistency with that from the observations. However, the region-specific and site-specific comparisons revealed that during the growing season, the isoprene mixing ratios are significantly overestimated by the model at most sites in the south but underestimated at most sites in the north. Additionally, the observations revealed similar levels of isoprene in northern and southern China, whereas the simulated isoprene concentrations were higher in the south than in the north than in the north. This north-south discrepancy in the measurement-model comparisons might be related to the rapid afforestation rate in the north (largely due to tree-planting programs and policies incentivizing returning farmland to forest) and rapid urbanization rate in the southeast, the subsequent inadequate characterization of isoprene-emitting tree species, and the lack of spatial representation in current models. Timely updates of high-resolution PFT and LAI data in MEGAN will be necessary. In the north, natural emissions of isoprene should reach their annual minimums during winter based on the model simulation. However, abnormally high ambient isoprene levels were measured in conjunction with high levels of combustion tracers, suggesting that there might be nonbiogenic sources in winter in the north, most probably coal/biomass combustion sources related to winter heating. Therefore, the nonbiogenic sources are necessary to be incorporated into the model to improve the simulation results in winter of the north China.

Measurement-model comparison for the highly reactive compound isoprene is challenging. In this study, we tried to make use of the best available observation data, and the measurement-model comparison results provided valuable information for the research communities studying biogenic emissions and atmospheric chemistry. However, the site-based samples in this study are still too sparse, and thus more field campaigns with higher spatial and temporal resolutions are necessary in future studies to further evaluate the uncertainty of isoprene emission estimates through the current model simulations. It is worth noting that most sites in this study are not in forested locations, more study on nontree biogenic isoprene emissions might help determine whether uncertainty in nontree biogenic emissions is also a factor influencing the model performance.

Data Availability Statement

The observed and simulated data used for this paper are available on request by writing to X. M. Wang (wangxm@gig.ac.cn) and at https://data.mendeley.com/datasets/3g4ptfktkt/2.

References

Andreae, M. O. (2019). Emission of trace gases and aerosols from biomass burning–An updated assessment. *Atmospheric Chemistry and Physics*, *19*, 8523–8546.

Arneth, A., Schurgers, G., Lathiere, J., Duhl, T., Beerling, D. J., Hewitt, C. N., et al. (2011). Global terrestrial isoprene emission models: Sensitivity to variability in climate and vegetation. *Atmospheric Chemistry and Physics*, *11*(15), 8037–8052.

Atkinson, R., & Arey, J. (1998). Atmospheric chemistry of biogenic organic compounds. *Accounts of Chemical Research*, *31*, 574–583.

Bai, J., Baker, B., Liang, B., Greenberg, J., & Guenther, A. (2006). Isoprene and monoterpene emissions from an Inner Mongolia grassland. *Atmospheric Environment*, *40*(30), 5753–5758.

Bai, J., Guenther, A., Turnipseed, A., & Duhl, T. (2015). Seasonal and interannual variations in whole-ecosystem isoprene and monoterpene emissions from a temperate mixed forest in Northern China. *Atmospheric Pollution Research*, *6*(4), 696–707.

Bai, J., Guenther, A., Turnipseed, A., Duhl, T., & Greenberg, J. (2017). Seasonal and interannual variations in whole-ecosystem BVOC emissions from a subtropical plantation in China. *Atmospheric Environment*, *161*, 176–190.

Bai, J., Guenther, A., Turnipseed, A., Duhl, T., Yu, S., & Wang, B. (2016). Seasonal variations in whole-ecosystem BVOC emissions from a subtropical bamboo plantation in China. *Atmospheric Environment*, *124*, 12–21.

Bai, J., Wang, G., Ren, L., Baker, B., Zimmerman, P., & Liang, B. (2003). The emission flux of volatile organic compounds in the Inner Mongolia Grassland. *Environmental Sciences*, *24*(6), 16–22.

Bey, I., Jacob, D. J., Yantosca, R. M., Logan, J. A., Field, B. D., Fiore, A. M., et al. (2001). Global modeling of tropospheric chemistry with assimilated meteorology: Model description and evaluation. *Journal of Geophysical Research*, *106*(D19), 23073–23095. https://doi.org/10.1029/2001JD000807

Borbon, A., Fontaine, H., Veillerot, M., Locoge, N., Galloo, J. C., & Guillermo, R. (2001). An investigation into the traffic-related fraction of isoprene at an urban location. *Atmospheric Environment*, *35*(22), 3749–3760. https://doi.org/10.1016/s1352-2310(01)00170-4

Butler, T. M., Taraborrelli, D., Fischer, C. B. H., Harder, H., Martinez, M., Williams, J., et al. (2008). Improved simulation of isoprene oxidation chemistry with the ECHAM5/MESSy chemistry-climate model: Lessons from the GABRIEL airborne field campaign. *Atmospheric Chemistry and Physics*, *8*(16), 4529–4546. https://doi.org/10.5194/acp-8-4529-2008

Carlton, A. G., & Baker, K. R. (2011). Photochemical modeling of the Ozark isoprene volcano: MEGAN, BEIS, and their impacts on air quality predictions. *Environmental Science & Technology*, *45*(10), 4438–4445. https://doi.org/10.1021/es200050x

Chameides, W. L., Lindsay, R. W., Richardson, J., & Kiang, C. S. (1988). The role of biogenic hydrocarbons in urban photochemical smog–Atlanta as a case study. *Science*, *241*(4872), 1473–1475. https://doi.org/10.1126/science.3420404

Chen, C., Park, T., Wang, X., Piao, S., Xu, B., Chaturvedi, R. K., et al. (2019). China and India lead in greening of the world through land-use management. *Nature Sustainability*, *2*, 122–129. https://doi.org/10.1038/s41893-019-0220-7

Chen, W. H., Guenther, A. B., Wang, X. M., Chen, Y. H., Gu, D. S., Chang, M., et al. (2018). Regional to global biogenic isoprene emission responses to changes in vegetation from 2000 to 2015. *Journal of Geophysical Research: Atmospheres*, *123*, 3757–3771.

Cheng, Y., Wang, Y., Zhang, Y., Chen, G., Crawford, J. H., Kleb, M. M., et al. (2017). Large biogenic contribution to boundary layer O_3-CO regression slope in summer. *Geophysical Research Letters*, *44*, 7061–7068. https://doi.org/10.1002/2017GL074405

Chi, Y., & Xie, S. (2011). Spatiotemporal inventory of biogenic volatile organic compound emissions in China based on vegetation volume and production. *Advanced Materials Research*, *356–360*, 2579–2582.

Choi, Y., Wang, Y., Yang, Q., Cunnold, D., Zeng, T., Shim, C., et al. (2008a). Spring to summer northward migration of high O_3 over the western North Atlantic. *Geophysical Research Letters*, *35*(4), 1–5. https://doi.org/10.1029/2007gl032276

Choi, Y., Wang, Y., Zeng, T., Cunnold, D., Yang, E.-S., Martin, R., et al. (2008b). Springtime transitions of NO_2, CO, and O_3 over North America: Model evaluation and analysis. *Journal of Geophysical Research*, *113*(D20), 1–16. https://doi.org/10.1029/2007jd009632

Claeys, M., Graham, B., Vas, G., Wang, W., Vermeylen, R., Pashynska, V., et al. (2004). Formation of secondary organic aerosols through photooxidation of isoprene. *Science*, *303*(5661), 1173–1176. https://doi.org/10.1126/science.1092805

Fang, Z., Deng, W., Zhang, Y., Ding, X., Tang, M., Liu, T., et al. (2017). Open burning of rice, corn and wheat straws: Primary emissions, photochemical aging, and secondary organic aerosol formation. *Atmospheric Chemistry and Physics*, *17*(24), 14821–14839. https://doi.org/10.5194/acp-17-14821-2017

Fang, J. Y., Song, Y. C., Liu, H. Y., & Piao, S. L. (2002). Vegetation-climate relationship and its application in the division of vegetation zone in China. *Acta Botanica Sinica*, *44*(9), 1105–1122.

Fehsenfeld, F., Calvert, J., Fall, R., Goldan, P., Guenther, A., Hewitt, C., et al. (1992). Emissions of volatile organic compounds from vegetation and their implications for atmospheric chemistry. *Global Biogeochemical Cycles*, *6*, 389–430.

Fujita, E. M., Campbell, D. E., Stockwell, W. R., & Lawson, D. R. (2013). Past and future ozone trends in California's South Coast Air Basin: Reconciliation of ambient measurements with past and projected emission inventories. *Journal of the Air and Waste Management Association*, *63*(1), 54–69. https://doi.org/10.1080/10962247.2012.735211

Fu, Y., & Liao, H. (2012). Simulation of the interannual variations of biogenic emissions of volatile organic compounds in China: Impacts on tropospheric ozone and secondary organic aerosol. *Atmospheric Environment*, *59*, 170–185. http://dx.doi.org/10.1016/j.atmosenv.2012.05.053

Fu, Y., & Liao, H. (2014). Impacts of land use and land cover changes on biogenic emissions of volatile organic compounds in China from the late 1980s to the mid-2000s: Implications for tropospheric ozone and secondary organic aerosol. *Tellus B: Chemical and Physical Meteorology*, *66*(1), 1–17. https://doi.org/10.3402/tellusb.v66.24987

Geron, C., Owen, S., Guenther, A., Greenberg, J., Rasmussen, R., Bai, J. H., et al. (2006). Volatile organic compounds from vegetation in southern Yunnan Province, China: Emission rates and some potential regional implications. *Atmospheric Environment*, *40*(10), 1759–1773.

Guenther, A., Hewitt, C.N., Erickson, D., Fall, R., Geron, C., Graedel, T., et al. (1995). A global model of natural volatile organic compound emissions. *Journal of Geophysical Research*, *100*(D5), 8873–8892. https://doi.org/10.1029/94jd02950

Guenther, A. B., Jiang, X., Heald, C. L., Sakulyanontvittaya, T., Duhl, T., Emmons, L. K., et al. (2012). The model of emissions of gases and aerosols from nature version 2.1 (MEGAN2.1): An extended and updated framework for modeling biogenic emissions. *Geoscientific Model Development*, *5*(6), 1471–1492. https://doi.org/10.5194/gmd-5-1471-2012

Guenther, A., Karl, T., Harley, P., Wiedinmyer, C., Palmer, P. I., & Geron, C. (2006). Estimates of global terrestrial isoprene emissions using MEGAN (Model of emissions of gases and aerosols from Nature). *Atmospheric Chemistry and Physics*, *6*, 3181–3210.

Guenther, A. B., Monson, R. K., & Fall, R. (1991). Isoprene and monoterpene emission rate variability-observations with eucalyptus and emission rate algorithm development. *Journal of Geophysical Research*, *96*(D6), 10799–10808. https://doi.org/10.1029/91jd00960

Guenther, A. B., Zimmerman, P. R., Harley, P. C., Monson, R. K., & Fall, R. (1993). Isoprene and monoterpene emission rate variability-model evaluations and sensitivity analysis. *Journal of Geophysical Research*, *98*(D7), 12609–12617. https://doi.org/10.1029/93jd00527

Hantson, S., Knorr, W., Schurgers, G., Pugh, T. A. M., & Arneth, A. (2017). Global isoprene and monoterpene emissions under changing climate, vegetation, CO_2 and land use. *Atmospheric Environment*, *155*, 35–45.

Henrot, A. J., Stanelle, T., Schröder, S., Siegenthaler, C., Taraborrelli, D., & Schultz, M. G. (2017). Implementation of the MEGAN (v2.1) biogenic emission model in the ECHAM6-HAMMOZ chemistry climate model. *Geoscientific Model Development*, *10*(2), 903–926.

Hewitt, C. N., Ashworth, K., Boynard, A., Guenther, A., Langford, B., MacKenzie, A. R., et al. (2011). Ground-level ozone influenced by circadian control of isoprene emissions. *Nature Geoscience*, *4*(10), 671–674. https://doi.org/10.1038/ngeo1271

Klinger, L. F., Li, Q. J., Guenther, A. B., Greenberg, J. P., Baker, B., & Bai, J. H. (2002). Assessment of volatile organic compound emissions from ecosystems of China. *Journal of Geophysical Research*, *107*(D21), ACH 16-11–ACH 16-21, 1–16. https://doi.org/10.1029/2001JD001076

Kota, S. H., Schade, G., Estes, M., Boyer, D., & Ying, Q. (2015). Evaluation of MEGAN predicted biogenic isoprene emissions at urban locations in Southeast Texas, *Atmospheric Environment*, *110*, 54–64. https://doi.org/10.1016/j.atmosenv.2015.03.027

Langford, A. O., Senff, C. J., Alvarez, R. J. II, Banta, R. M., & Hardesty, R. M. (2010). Long-range transport of ozone from the Los Angeles basin: A case study. *Geophysical Research Letters*, *37*(L06807), 1–5. https://doi.org/10.1029/2010gl042507

Lathière, J., Hewitt, C. N., & Beerling, D. J. (2010). Sensitivity of isoprene emissions from the terrestrial biosphere to 20th century changes in atmospheric CO_2 concentration, climate, and land use. *Global Biogeochemical Cycles*, *24*, GB1004. https://doi.org/10.1029/2009GB003548

Lelieveld, J., Butler, T. M., Crowley, J. N., Dillon, T. J., Fischer, H., Ganzeveld, L., et al. (2008). Atmospheric oxidation capacity sustained by a tropical forest. *Nature*, *452*(7188), 737–740. https://doi.org/10.1038/nature06870

Li, L. Y., Chen, Y., & Xie, S. D. (2013). Spatio-temporal variation of biogenic volatile organic compounds emissions in China. *Environmental Pollution*, *182*, 157–168. http://dx.doi.org/10.1016/j.envpol.2013.06.042

Li, M., Zhang, Q., Kurokawa, J.-I., Woo, J.-H., He, K., Lu, Z., et al. (2017). MIX: A mosaic Asian anthropogenic emission inventory under the international collaboration framework of the MICS-Asia and HTAP. *Atmospheric Chemistry and Physics*, *17*, 935–963. https://doi.org/10.5194/acp-17-935-2017

Li, J., Hao, Y., Simayi, M., Shi, Y., Xi, Z., & Xie, S. (2019). Verification of anthropogenic VOC emission inventory through ambient measurements and satellite retrievals. *Atmospheric Chemistry and Physics*, *19*(9), 5905–5921. https://doi.org/10.5194/acp-19-5905-2019

Liu, Z., Wang, Y., Gu, D., Zhao, C., Huey, L. G., Stickel, R., et al. (2010). Evidence of reactive aromatics as a major source of peroxy acetyl nitrate over China. *Environmental Science & Technology*, *44*(18), 7017–7022.

Liu, Z., Wang, Y., Gu, D., Zhao, C., Huey, L. G., Stickel, R., et al. (2012a). Summertime photochemistry during CAREBeijing-2007: ROx budgets and O_3 formation. *Atmospheric Chemistry and Physics*, *12*(16), 7737–7752.

Liu, Z., Wang, Y., Vrekoussis, M., Richter, A., Wittrock, F., Burrows, J. P., et al. (2012b). Exploring the missing source of glyoxal (CHOCHO) over China. *Geophysical Research Letters*, *39*(L10812), 1–5. https://doi.org/10.1029/2012GL051645

Liu, C., Ma, Z., Mu, Y., Liu, J., Zhang, C., Zhang, Y., et al. (2017a). The levels, variation characteristics, and sources of atmospheric non-methane hydrocarbon compounds during wintertime in Beijing, China. *Atmospheric Chemistry and Physics*, *17*(17), 10633–10649. https://doi.org/10.5194/acp-17-10633-2017

Liu, C., Zhang, C., Mu, Y., Liu, J., & Zhang, Y. (2017b). Emission of volatile organic compounds from domestic coal stove with the actual alternation of flaming and smoldering combustion processes. *Environmental Pollution*, *221*, 385–391. https://doi.org/10.1016/j.envpol.2016.11.089

Li, J. F., Wang, Y. H., & Qu, H. (2019). Dependence of summertime surface ozone on NOx and VOC emissions over the United States: Peak time and value. *Geophysical Research Letters*, *46*(6), 3540–3550. https://doi.org/10.1029/2018gl081823

Li, L. Y., & Xie, S. D. (2014). Historical variations of biogenic volatile organic compound emission inventories in China, 1981–2003. *Atmospheric Environment*, *95*, 185–196. http://dx.doi.org/10.1016/j.atmosenv.2014.06.033

Li, L., Yang, W., Xie, S., & Wu, Y. (2020). Estimations and uncertainty of biogenic volatile organic compound emission inventory in China for 2008–2018. *The Science of the Total Environment*, *733*, 139301.

Ng, N. L., Kwan, A. J., Surratt, J. D., Chan, A. W. H., Chhabra, B. S., Sorooshian, A., et al. (2008). Secondary organic aerosol (SOA) formation from reaction of isoprene with nitrate radicals (NO₃). *Atmospheric Chemistry and Physics*, *8*(14), 4117–4140. https://doi.org/10.5194/acp-8-4117-2008

Otu-Larbi, F. C., Bolas, V., Ferracci, Z., Staniaszek, R., Jones, Y., Mahli, N., et al. (2019). Modelling the effect of the 2018 summer heatwave and drought on isoprene emissions in a UK woodland: Modelling isoprene emissions during heatwave-drought. *Global Change Biology*, 2320–2335. https://doi.org/10.1111/GCB.14963

Park, C., Schade, G. W., & Boedeker, I. (2011). Characteristics of the flux of isoprene and its oxidation products in an urban area. *Journal of Geophysical Research*, *116*(D21303), 1–13. https://doi.org/10.1029/2011jd015856

Paulot, F., Crounse, J. D., Kjaergaard, H. G., Kurten, A., St Clair, J. M., Seinfeld, J. H., et al. (2009). Unexpected epoxide formation in the gas-phase photooxidation of isoprene. *Science*, *325*(5941), 730–733. https://doi.org/10.1126/science.1172910

Paulot, F., Henze, D. K., & Wennberg, P. O. (2012). Impact of the isoprene photochemical cascade on tropical ozone. *Atmospheric Chemistry and Physics*, *12*(3), 1307–1325. https://doi.org/10.5194/acp-12-1307-2012

Pierce, T., Geron, C., Bender, L., Dennis, R., Tonnesen, G., & Guenther, A. (1998). Influence of increased isoprene emissions on regional ozone modeling. *Journal of Geophysical Research*, *103*, 25611–25629.

Saha, S., Moorthi, S., Pan, P. L., Wu, X., Wang, J., Nadiga, S., et al. (2010). The NCEP climate forest system reanalysis. *Bulletin of the American Meteorological Society*, *91*(8), 1015–1057. https://doi.org/10.1175/2010bams3001.1

Seinfeld, J. H., & Pandis, S. N. (1998). *Atmospheric Chemistry and Physics: From air pollution to climate change*. New York, NY: John Wiley & Sons Inc.

Simpson, I. J., Akagi, S. K., Barletta, B., Blake, N. J., Choi, J., Diskin, D. S., et al. (2011). Boreal forest fire emissions in fresh Canadian smoke plumes: C_1-C_{10} volatile organic compounds (VOCs), CO_2, CO, NO_2, NO, HCN and CH_3CN. *Atmospheric Chemistry and Physics*, *11*(13), 6445–6463. https://doi.org/10.5194/acp-11-6445-2011

Situ, S., Guenther, A., Wang, X., Jiang, X., Turnipseed, A., Wu, Z., et al. (2013). Impacts of seasonal and regional variability in biogenic VOC emissions on surface ozone in the Pearl River delta region, China. *Atmospheric Chemistry and Physics*, *13*(23), 11803–11817. https://doi.org/10.5194/acp-13-11803-2013

Situ, S., Wang, X. M., Guenther, A., Zhang, Y. L., Wang, X. M., Huang, M. J., et al. (2014). Uncertainties of isoprene emissions in the MEGAN model estimated for a coniferous and broad-leaved mixed forest in Southern China. *Atmospheric Environment*, *98*, 105–110. https://doi.org/10.1016/j.atmosenv.2014.08.023

Song, J., Vizuete, W., Chang, S., Allen, D., Kimura, Y., Kemball–Cook, S., et al. (2008). Comparisons of modeled and observed isoprene concentrations in southeast Texas. *Atmospheric Environment*, *42*(8), 1922–1940. https://doi.org/10.1016/j.atmosenv.2007.11.016

Starn, T. K., Shepson, P. B., Bertman, S. B., White, J. S., Splawn, B. G., Riemer, D. D., et al. (1998). Observations of isoprene chemistry and its role in ozone production at a semirural site during the 1995 Southern Oxidants Study. *Journal of Geophysical Research*, *103*(D17), 22425–22435. https://doi.org/10.1029/98jd01279

Surratt, J. D., Chan, A. W. H., Eddingsaas, N. S., Chan, M., Loza, C. L., Kwan, A. J., et al. (2010). Reactive intermediates revealed in secondary organic aerosol formation from isoprene. *Proceedings of the National Academy of Sciences of the United States of America*, *107*(15), 6640–6645. https://doi.org/10.1073/pnas.0911114107

Tai, A. P. K., Mickley, L. J., Heald, C. L., & Wu, S. L. (2013). Effect of CO_2 inhibition on biogenic isoprene emission: Implications for air quality under 2000 to 2050 changes in climate, vegetation, and land use. *Geophysical Research Letters*, *40*(13), 3479–3483. https://doi.org/10.1002/grl.50650

Tie, X. X., Li, G. H., Ying, Z. M., Guenther, A., & Madronich, S. (2006). Biogenic emissions of isoprenoids and NO in China and comparison to anthropogenic emissions. *The Science of the Total Environment*, *371*(1–3), 238–251. https://doi.org/10.1016/j.scitotenv.2006.06.025

Unger, N. (2013). Isoprene emission variability through the twentieth century. *Journal of Geophysical Research Atmospheres*, *118*(24), 13606–13613. https://doi.org/10.1002/2013JD020978

Unger, N. (2014). Human land-use-driven reduction of forest volatiles cools global climate. *Nature Climate Change*, *4*(10), 907–910.

von Kuhlmann, R., Lawrence, M. G., Poschl, U., & Crutzen, P. J. (2004). Sensitivities in global scale modeling of isoprene. *Atmospheric Chemistry and Physics*, *4*, 1–17.

Wang, Y., Brandt, M., Zhao, M., Tong, X., Xing, K., Xue, F., et al. (2018b). Major forest increase on the Loess Plateau, China (2001-2016). *Land Degradation & Development*, *29*(11), 4080–4091.

Wang, Y. H., Jacob, D. J., & Logan, J. A. (1998). Global simulation of tropospheric O_3-NOx-hydrocarbon chemistry 3. Origin of tropospheric ozone and effects of nonmethane hydrocarbons. *Journal of Geophysical Research*, *103*(D9), 10757–10767. https://doi.org/10.1029/98jd00156

Wang, P., Schade, G., Estes, M., & Ying, Q. (2017a). Improved MEGAN predictions of biogenic isoprene in the contiguous United States. *Atmospheric Environment*, *148*, 337–351. https://doi.org/10.1016/j.atmosenv.2016.11.006

Wang, X. M., Situ, S. P., Guenther, A., Chen, F., Wu, Z. Y., Xia, B. C., et al. (2011). Spatiotemporal variability of biogenic terpenoid emissions in Pearl River Delta, China, with high-resolution land-cover and meteorological data. *Tellus B: Chemical and Physical Meteorology*, *63*(2), 241–254. https://doi.org/10.1111/j.1600-0889.2010.00523.x

Wang, H., Wu, Q., Liu, H., Wang, Y., Cheng, H., Wang, R., et al. (2018a). Sensitivity of biogenic volatile organic compound emissions to leaf area index and land cover in Beijing. *Atmospheric Chemistry and Physics*, *18*(13), 9583–9596.

Wang, T., Xue, L., Brimblecombe, P., Lam, Y. F., Li, L., & Zhang, L. (2017b). Ozone pollution in China: A review of concentrations, meteorological influences, chemical precursors, and effects. *The Science of the Total Environment*, *575*, 1582–1596. https://doi.org/10.1016/j.scitotenv.2016.10.081

Wang, Y., Zhao, Y., Zhang, L., Zhang, J., & Liu, Y. (2020). Modified regional biogenic VOC emissions with actual ozone stress and integrated land cover information: A case study in Yangtze River Delta, China. *The Science of the Total Environment*, *727*, 138703.

Warneke, C., de Gouw, J. A., Del Negro, L., Brioude, J., McKeen, S., Stark, H., et al. (2010). Biogenic emission measurement and inventories determination of biogenic emissions in the eastern United States and Texas and comparison with biogenic emission inventories. *Journal of Geophysical Research: Atmospheres*, *115*(D00F18), 1–21. https://doi.org/10.1029/2009jd012445

Wei, C., Lu, J., Xu, L., Liu, G., Wang, Z., Zhao, F., et al. (2014). Genetic structure of Chinese indigenous goats and the special geographical structure in the southwest China as a geographic barrier driving the fragmentation of a large population. *PLoS One*, *9*(4), 1–12. https://doi.org/10.1371/journal.pone.0094435

Xin, J., Wang, Y., Pan, Y., Ji, D., Liu, Z., Wen, T., et al. (2015). The campaign on atmospheric aerosol research network of China: CARE-China. *Bulletin of the American Meteorological Society*, *96*(7), 1137–1155.

Yan, M., Chan, J. C. L., and Zhao, K. (2020), Impacts of urbanization on the precipitation characteristics in Guangdong Province, China, *Advances in Atmospheric Sciences, 37*(7), 696–706.

Yang, W., Zhang, Y., Wang, X., Li, S., Zhu, M., Yu, Q., et al. (2018). Volatile organic compounds at a rural site in Beijing: Influence of temporary emission control and wintertime heating. *Atmospheric Chemistry and Physics*, *18*(17), 12663–12682. https://doi.org/10.5194/acp-18-12663-2018

Ying, Q., Li, J., & Kota, S. H. (2015). Significant contributions of isoprene to summertime secondary organic aerosol in eastern United States. *Environmental Science & Technology*, *49*(13), 7834–7842. https://doi.org/10.1021/acs.est.5b02514

Yin, L., Xu, Z., Liu, M., Xu, T., Wang, T., Liao, W., et al. (2020). Estimation of biogenic volatile organic compound (BVOC) emissions in China using WRF–CLM–MEGAN coupled model. *Biogeosciences Discussions*, *2020*, 1–30.

Zhang, Y. L., Wang, X., Blake, D. R., Li, L., Zhang, Z., Wang, S., et al. (2012). Aromatic hydrocarbons as ozone precursors before and after outbreak of the 2008 financial crisis in the Pearl River Delta region, south China. *Journal of Geophysical Research*, *117*, D15306. https://doi.org/10.1029/2011JD017356

Zhang, Y. L., Wang, X., Barletta, B., Simpson, I. J., Blake, D. R., Fu, X., et al. (2013). Source attributions of hazardous aromatic hydrocarbons in urban, suburban and rural areas in the Pearl River Delta (PRD) region. *Journal of Hazardous Materials*, *250*, 403–411. https://doi.org/10.1016/j.jhazmat.2013.02.023

Zhang, Y., Wang, Y., Chen, G., Smeltzer, C., Crawford, J., Olson, J., et al. (2016a). Large vertical gradient of reactive nitrogen oxides in the boundary layer: Modeling analysis of DISCOVER-AQ 2011 observations. *Journal of Geophysical Research: Atmospheres*, *120*. https://doi.org/10.1002/2015JD024203

Zhang, R., Wang, Y., He, Q., Chen, L., Zhang, Y., Qu, H., et al. (2017). Enhanced trans-Himalaya pollution transport to the Tibetan Plateau by cut-off low systems. *Atmospheric Chemistry and Physics*, *17*(4), 3083–3095. https://doi.org/10.5194/acp-17-3083-2017

Zhang, X., Huang, T., Zhang, L., Shen, Y., Zhao, Y., Gao, H., et al. (2016). Three-North Shelter Forest Program contribution to long-term increasing trends of biogenic isoprene emissions in northern China. *Atmospheric Chemistry and Physics*, *16*(11), 6949–6960. https://doi.org/10.5194/acp-16-6949-2016

Zhang, Y., & Wang, Y. (2016). Climate-driven ground-level ozone extreme in the fall over the Southeast United States. *Proceedings of the National Academy of Sciences of the United States of America*, *113*(36), 10025–10030. https://doi.org/10.1073/pnas.1602563113

Zhang, R. X., Wang, Y., Smeltzer, C., Qu, H., Koshak, W., & Boersma, K. F. (2018). Comparing OMI-based and EPA AQS in situ NO_2 trends: Towards understanding surface NOx emission changes. *Atmospheric Measurement Techniques*, *11*(7), 3955–3967. https://doi.org/10.5194/amt-11-3955-2018

Zhang, Z., Wang, X., Zhang, Y., Lü, S., Huang, Z., Huang, X., et al. (2015). Ambient air benzene at background sites in China's most developed coastal regions: Exposure levels, source implications and health risks. *The Science of the Total Environment*, *511*, 792–800.

Zhang, Z., Zhang, Y., Wang, X., Lu, S., Huang, Z., Huang, X., et al. (2016b). Spatiotemporal patterns and source implications of aromatic hydrocarbons at six rural sites across China's developed coastal regions. *Journal of Geophysical Research: Atmospheres*, *121*(11), 6669–6687. https://doi.org/10.1002/2016JD025115

Zhao, C., Wang, Y., Yang, Q., Fu, R., Cunnold, D., & Choi, Y. (2010). Impact of East Asian summer monsoon on the air quality over China: View from space. *Journal of Geophysical Research: Atmospheres*, *115*(D09301), 1–12. https://doi.org/10.1029/2009jd012745

Zhou, Y., Kong, Y., Wang, H., & Luo, F. (2020). The impact of population urbanization lag on eco-efficiency: A panel quantile approach. *Journal of Cleaner Production*, *244*, 118664.